

June 19, 2004  
IISc-CTS-02/02

## CP Violation in the Production of $\tau$ -Leptons at TESLA with Beam Polarization

**B. Ananthanarayan**

Centre for Theoretical Studies, Indian Institute of Science,  
Bangalore 560 012, India

**Saurabh D. Rindani**

Theory Group, Physical Research Laboratory,  
Navrangpura, Ahmedabad 380 009, India

**Achim Stahl**

DESY, Platanenallee 6,  
15738 Zeuthen, Germany

### Abstract

We study the prospects of discovering CP-violation in the production of  $\tau$  leptons in the reaction  $e^+e^- \rightarrow \tau^+\tau^-$  at TESLA, an  $e^+e^-$  linear collider with center-of-mass energies of 500 or even 800 GeV. Non-vanishing expectation values of certain correlations between the momenta of the decay products of the two  $\tau$  leptons would signal the presence of CP-violation beyond the standard model. We study how longitudinal beam polarization of the electron and positron beams will enhance these correlations. We find that T-odd and T-even vector correlations are well suited for the measurements of the real and imaginary parts of the electric dipole form factors. We expect measurements of the real part with a precision of roughly  $10^{-20}$  e-cm and of the imaginary part of  $10^{-17}$  e-cm. This compares well with the size of the expected effects in many extensions of the standard model.

# 1 Introduction

One possible signal for physics beyond the standard model (SM) would be the presence of significant CP violation in the production of  $\tau$  leptons [1, 2], or in their decay [3]. CP violation in production would arise, assuming that  $e^+e^-$  annihilate into a virtual  $\gamma$  or  $Z$ , from the electric dipole form factor (EDM)  $d_\tau^\gamma(q^2)$ , or its generalization for the  $Z$  coupling, the so-called “weak” dipole moment form factor (WDM)  $d_\tau^Z(q^2)$ . These are expected to be unobservably small in the SM. Thus, observation of CP violation in production would be unambiguous evidence for physics beyond the SM. The signal for CP violation in  $\tau$  production would be the non-zero values of certain momentum correlations of the  $\tau$  decay products [1, 2] since the momenta play the role of spin analyzers for the  $\tau$  leptons.

TESLA is a proposed  $e^+e^-$  linear collider with a center-of-mass energy of  $\sqrt{s} = 500$  GeV with the possibility of an extension to 800 GeV [4]. It is a multi-purpose machine that will test various aspects of the standard model (SM) and search for signals of interactions beyond the standard model. A strong longitudinal polarization program at TESLA with considerable polarization of the electron beam, with the possibility of some although not as high a degree of polarization of the positron beam is also planned [5]. We assume an integrated luminosity of a few hundred  $\text{fb}^{-1}$ , which would lead to copious production of  $\tau^+\tau^-$  pairs. Longitudinal beam polarization of the electron and positron beams would lead to a substantial enhancement of certain vector correlations, which are non-vanishing in the event that the  $\tau$  lepton has an EDM or a WDM. We will assume integrated luminosities of 500 and 1000  $\text{fb}^{-1}$  at center of mass energies of 500 and 800 GeV, respectively. We expect a magnitude of polarization of 80 % for the electron beam and 60 % for the positron beam.

Our aim in this work is to study these vector correlations constructed from the momenta of the charged decay products of  $\tau$  leptons. We will confine our attention to two-body decays of the  $\tau$  leptons for which the correlations as well as their variance due to CP conserving standard model interactions can be computed analytically. We also study the effects of helicity-flip bremsstrahlung [6] which contributes to these correlations at  $\mathcal{O}(\alpha)$ . This is a standard model background to the signal of interest.

The plan of the paper is the following: in the next section we present estimates for the EDM and WDM in certain popular extensions of the SM which sets the scale for our studies. In Sec. 3, we discuss the correlations in general and reproduce results from the literature for our vector correlations. In Sec. 4, we discuss the numerical results for TESLA energies, luminosities, and polarizations, including the limits achievable. In Sec. 6 we discuss the

implications of our results for the configuration being planned at TESLA and how our results will translate into certain design criteria for the machine and the detector.

## 2 Dipole Moments in Extensions to the Standard Model

CP violating dipole moments of leptons can arise in the standard model radiatively. However, since there is no CP violation in the lepton sector in SM, it can only be induced by CP violation in the quark sector. One has to go at least to 3-loop order to generate a non-vanishing contribution to the lepton dipole moments [7, 8]. A crude estimate gives

$$|d_\tau(SM)| \lesssim 10^{-34} \text{ e-cm.} \quad (1)$$

Extensions of the SM where complex couplings appear can easily generate CP-violating dipole moments for  $\tau$  lepton at one-loop order. Provided these couplings are generation or mass dependent, it is possible that reasonably large dipole moments for the  $\tau$  lepton are generated, while continuing to satisfy the constraints coming from strong limits on the electric dipole moments of the electron or the neutron.

Since dipole couplings of fermions are chirality flipping, they would be proportional to a fermionic mass. However, this need not necessarily be the mass of the  $\tau$  lepton. It could be the mass of some other heavy fermion in the theory. As a result, the dipole coupling at energy of  $\sqrt{s}$  need not necessarily be suppressed by a factor of  $m_\tau/\sqrt{s}$ , but could involve a factor  $m_F/\sqrt{s}$ , where  $F$  is a new heavy particle in the extension of the SM, and this factor need not be small. It is thus possible to get dipole form factors almost of the order of  $(\alpha/\pi)$  in units of an inverse mass which appears in the loop. If the mass is that of  $W$  or  $Z$ , it is possible to get dipole moments of the order of  $10^{-19}$  e-cm. In actual practice, however, the particle appearing in the loop is also constrained to be heavy. As a result, the dipole moments in left-right symmetric models, Higgs exchange model with spontaneous CP violation and natural flavor conservation, and supersymmetric models turn out to be of the order of  $10^{-23}$  e-cm, or smaller [7].

In the case of most models, information exists in the literature for the values of electric and weak dipole form factors only at  $q^2$  values of 0 and  $m_\tau^2$ , respectively. Models in which the  $q^2$  dependence of the CP-violating form factors has been studied are scalar leptoquark models with couplings only to the third generation of quarks and leptons. Of these, the most promising

model is the one in which the leptoquark transforms as an  $SU(2)$  doublet. In [9] a value of  $\text{Re } d_\tau^\gamma \lesssim 3 \cdot 10^{-19}$  e-cm was found above the  $Z$  resonance, with  $\text{Re } d_\tau^Z$  about  $\frac{1}{4}$  of this value for a more favorable case. Taking into account restrictions on the doublet leptoquark mass and couplings coming from LEP data values of  $d_\tau^\gamma \lesssim 10^{-19}$  e-cm and  $d_\tau^Z \lesssim (\text{few}) \cdot 10^{-20}$  e-cm were estimated at  $\sqrt{q^2} = 500$  GeV [10].

Values of  $\tau$  dipole form factors of the order of  $10^{-19}$  e-cm are also obtained in models with Majorana neutrinos of mass of a few hundred GeV, and of the order of  $10^{-20}$  e-cm in two-Higgs doublet extensions with natural flavor conservation, and in supersymmetric models through a complex  $\tau - \tilde{\tau}$ -neutralino coupling, not far from the  $\tilde{\tau}$  threshold [9].

### 3 The Vector Correlations

In ref. [1] an extensive analysis of momentum correlations was first presented in the context of the reaction  $e^+e^- \rightarrow Z^0 \rightarrow \tau^+\tau^-$ , and was subsequently generalized to energies far away from the  $Z$  resonance in [2]. Expressions were presented there for the  $\tau$  production matrix  $\chi$  involving the EDM and the WDM, in addition to the main contribution from SM vertices, which is required to compute the production cross-section, the momentum correlations of interest, as well as their variances, also taking into account the  $\mathcal{D}$  matrices that account for the decay of the  $\tau$  into (two-body) final states. In ref. [11] it was shown that in the limit of vanishing electron mass, the initial state depends on the electron polarization  $P_e$  and the positron polarization  $P_{\bar{e}}$  only through the CP-even combinations  $(P_e - P_{\bar{e}})$  and  $(1 - P_e P_{\bar{e}})$ . Therefore one may search for CP violation through the non-vanishing expectation values of CP-odd momentum correlations for arbitrary electron and positron polarizations. In particular, simple “vector” correlations for which the correlations as well as their variances could be computed in closed form, were shown to have enhanced sensitivity to CP violating EDM and WDM of the  $\tau$  leptons at SLC, and at the energies of a Tau-charm factory. In this work, we shall examine these correlations for their sensitivity to  $\tau$  EDM and WDM at TESLA energies, polarizations and luminosities.

The CP-odd momentum correlations we consider here are associated with the center of mass momenta  $\mathbf{q}_{\bar{B}}$  of  $\bar{B}$  and  $\mathbf{q}_A$  of  $A$ , where the  $\bar{B}$  and  $A$  arise in the decays  $\tau^+ \rightarrow \bar{B}\bar{\nu}_\tau$  and  $\tau^- \rightarrow A\nu_\tau$ , and where  $A, B$  run over  $\pi, \rho, a_1$ , etc. In the case when  $A$  and  $B$  are different, one has to consider also the decays with  $A$  and  $B$  interchanged, so as to construct correlations which are explicitly CP-odd.

The correlations we consider are

$$O_1 \equiv \frac{1}{2} [\hat{\mathbf{p}} \cdot (\mathbf{q}_{\overline{B}} \times \mathbf{q}_A) + \hat{\mathbf{p}} \cdot (\mathbf{q}_{\overline{A}} \times \mathbf{q}_B)] \quad (2)$$

and

$$O_2 \equiv \frac{1}{2} [\hat{\mathbf{p}} \cdot (\mathbf{q}_A + \mathbf{q}_{\overline{B}}) + \hat{\mathbf{p}} \cdot (\mathbf{q}_{\overline{A}} + \mathbf{q}_B)], \quad (3)$$

where  $\hat{\mathbf{p}}$  is the unit vector in the positron beam direction.

Note that since  $O_2$  is CPT-odd it measures  $\text{Im } d_\tau^i$ , whereas  $O_1$  is CP-even and measures  $\text{Re } d_\tau^i$ . An additional advantage of these correlations is that the correlations as well as the standard deviation for the operators due to the standard model background are both calculable in closed form for two-body decays of the  $\tau$  leptons.

The calculations include two-body decay modes of the  $\tau$  in general and are applied specifically to the case of  $\tau \rightarrow \pi \nu_\tau$  and  $\tau \rightarrow \rho \nu_\tau$  due to the fact that these modes possess a good resolving power of the  $\tau$  polarization, parameterized in terms of the constant  $\alpha_\pi = 1$  for the  $\pi$  channel (with branching fraction of about 11%) and  $\alpha_\rho = 0.46$  for the  $\rho$  channel (with branching fraction of about 25%) from the momentum of the  $\pi$  or the  $\rho$ .

Analytic expressions for these correlations can be found in [12]. For the sake of convenience of reference and completeness, we give the expressions here. With the definitions  $r_{ij} \equiv (V_e^i A_e^j + V_e^j A_e^i)/(V_e^i V_e^j + A_e^i A_e^j)$  and the effective polarization parameter  $P \equiv (P_e - P_{\overline{e}})/(1 - P_e P_{\overline{e}})$  (the vector and axial-vector couplings  $A_l^i, V_l^i, l = e$  or  $\tau, i = \gamma$  or  $Z$  are listed in [2]),

$$\begin{aligned} \langle O_1 \rangle = & -\frac{1}{36x\sigma} \sum_{i,j} K_{ij} s^{3/2} m_\tau^2 (1-x^2) \left( \frac{r_{ij}-P}{1-r_{ij}P} \right) \\ & [(A_\tau^i \text{Re } d_\tau^j + A_\tau^j \text{Re } d_\tau^i) \alpha_A \alpha_B (1-p_A)(1-p_B) - \\ & \frac{3}{2} (V_\tau^i \text{Re } d_\tau^j + V_\tau^j \text{Re } d_\tau^i) [\alpha_A(1-p_A)(1+p_B) + \alpha_B(1-p_B)(1+p_A)], \end{aligned} \quad (4)$$

and

$$\begin{aligned} \langle O_2 \rangle = & \frac{1}{3\sigma} \sum_{i,j} K_{ij} s^{3/2} m_\tau \left( \frac{r_{ij}-P}{1-r_{ij}P} \right) \\ & \frac{1}{4} (A_\tau^i \text{Im } d_\tau^j + A_\tau^j \text{Im } d_\tau^i) (1-x^2) (\alpha_A(1-p_A) + \alpha_B(1-p_B)), \end{aligned} \quad (5)$$

where  $x = 2m_\tau/\sqrt{s}$ ,  $p_{A,B} = m_{A,B}^2/m_\tau^2$ , and  $\sigma$  is the cross-section of  $e^+e^- \rightarrow \tau^+\tau^-$  given by:

$$\sigma = \sum_{i,j} K_{ij} s [V_\tau^i V_\tau^j (1 + \frac{x^2}{2}) + A_\tau^i A_\tau^j (1 - x^2)], \quad (6)$$

and

$$K_{ij} = \frac{(V_e^i V_e^j + A_e^i A_e^j)(1 - r_{ij}P)}{12\pi(s - M_i^2)(s - M_j^2)} (1 - x^2)^{1/2} [1 - P_e P_{\overline{e}}]. \quad (7)$$

Since the energies involved are far above the  $Z$  resonance, we have neglected the  $Z$  width in the expressions above.

We have analytic expressions for the variance  $S_a^2 \equiv \langle O_a^2 \rangle - \langle O_a \rangle^2 \approx \langle O_a^2 \rangle$  in each case, arising from the CP-invariant SM part of the interaction:

$$\begin{aligned}
\langle O_1^2 \rangle = & \frac{1}{720x^2\sigma} \sum_{i,j} K_{ij} sm_\tau^4 \left( (1-p_A)^2(1-p_B)^2 \right. \\
& [V_\tau^i V_\tau^j (6+8x^2+x^4) + A_\tau^i A_\tau^j (6-2x^2-4x^4)] \\
& + (1-x^2) \left( [(1+p_A)^2(1-p_B)^2 + (1+p_B)^2(1-p_A)^2] \right. \\
& [3V_\tau^i V_\tau^j (3+2x^2) + 9A_\tau^i A_\tau^j (1-x^2)] \\
& + 4\alpha_A \alpha_B (1-p_B^2)(1-p_A^2)(1-x^2) [V_\tau^i V_\tau^j - A_\tau^i A_\tau^j] \\
& \left. \left. - 6(1-p_A)(1-p_B)(V_\tau^i A_\tau^j + V_\tau^j A_\tau^i)(1-x^2)(1-\frac{x^2}{6}) \right. \right. \\
& \left. \left. [\alpha_A(1+p_A)(1-p_B) + \alpha_B(1+p_B)(1-p_A)] \right) \right), \tag{8}
\end{aligned}$$

$$\begin{aligned}
\langle O_2^2 \rangle = & \frac{1}{360x^2\sigma} \sum_{i,j} K_{ij} sm_\tau^2 \\
\left[ \left( 3[(1-p_A)^2 + (1-p_B)^2] [V_\tau^i V_\tau^j (4+7x^2+4x^4) + A_\tau^i A_\tau^j 2(1-x^2)(2+3x^2)] \right. \right. \\
& \left. \left. - 2\alpha_A \alpha_B (1-p_A)(1-p_B) [V_\tau^i V_\tau^j (4+7x^2+4x^4) + A_\tau^i A_\tau^j 4(1-x^2)^2] \right) \right. \\
& \left. + 6 \left( 6(1-x^2)(p_A-p_B)^2 [V_\tau^i V_\tau^j (1+\frac{x^2}{4}) + A_\tau^i A_\tau^j (1-x^2)] \right. \right. \\
& \left. \left. - (V_\tau^i A_\tau^j + V_\tau^j A_\tau^i)(1-x^2)(4+x^2)(p_A-p_B) [\alpha_A(1-p_A) - \alpha_B(1-p_B)] \right) \right]. \tag{9}
\end{aligned}$$

The expected uncertainty (1 standard deviation) on the measurement of  $d_\tau$  can then be calculated from

$$\delta \text{Re(Im)} d_\tau^i = \frac{1}{c_{AB}^{a,i}} \frac{e}{\sqrt{s}} \frac{1}{\sqrt{N_{AB}}} S_a, \quad \begin{aligned} a &= 1(\text{Re}), 2(\text{Im}), \\ i &= \gamma, Z. \end{aligned} \tag{10}$$

The electric charge of the electron is denoted by  $e$ . The coefficients  $c_{AB}^{a,i}$  are discussed in the next section.  $N_{AB}$  is the number of events in the channel  $A\bar{B}$  and  $\bar{A}B$ , and is given by

$$N_{AB} = N_{\tau^+\tau^-} B(\tau^- \rightarrow A\nu_\tau) B(\tau^+ \rightarrow \bar{B}\bar{\nu}_\tau), \tag{11}$$

where we compute  $N_{\tau^+\tau^-}$  for the design luminosities and from the cross-section at the given energy and the polarizations.

$\sqrt{s}$ (GeV)	$\sigma_1$ (fb)	$\sigma_2$ (fb)
500	447.70	-31.37
800	174.03	-11.94

Table 1: Coefficients for the cross-section in fb for energies of interest

## 4 Results for TESLA

Here we present the results for the vector correlations and their standard deviation at TESLA energies, luminosities and polarizations, using the expressions of the previous section.

We begin with the expression for the cross-section which is of the form

$$\sigma_1(1 - P_e P_{\bar{e}}) + \sigma_2(P_e - P_{\bar{e}}) \quad (12)$$

The values of  $\sigma_1$  and  $\sigma_2$  for the energies of interest are given in Table 1. Furthermore, in Fig. 1 and Fig. 2 we present profiles of the cross-sections as a function for  $P_e$  where the profiles correspond to constant values of the positron polarization  $P_{\bar{e}} = 0, 0.3$  and  $0.6$ . We will, for the rest of the discussion, consider these to be the reference polarizations for the positron beam. Notice that the cross-section is larger when the  $e^+$  and  $e^-$  polarizations are opposite in sign, and then, it increases with  $e^+$  polarization. This results in better sensitivities for the corresponding cases.

Analogously, the expressions for the quantities  $c_{AB}^{a,i}$  and  $\langle O_a^2 \rangle$  may be schematically expressed as:

$$c_{AB}^{a,i} = f \frac{C_1^{a,i}(1 - P_e P_{\bar{e}}) + C_2^{a,i}(P_e - P_{\bar{e}})}{\sigma_1(1 - P_e P_{\bar{e}}) + \sigma_2(P_e - P_{\bar{e}})}, \quad \begin{array}{l} a = 1, 2 \\ i = \gamma, Z \end{array} \quad (13)$$

and

$$\langle O_a^2 \rangle = f \frac{D_1^a(1 - P_e P_{\bar{e}}) + D_2^a(P_e - P_{\bar{e}})}{\sigma_1(1 - P_e P_{\bar{e}}) + \sigma_2(P_e - P_{\bar{e}})}, \quad a = 1, 2. \quad (14)$$

respectively for the operators  $O_1$  and  $O_2$ , where  $f = 4\pi\alpha^2(\hbar c)^2/3 = 9.818 \cdot 10^7$  GeV<sup>2</sup>·fb. We have taken  $\alpha^{-1} = 128.87$ . The quantities  $C_k^{a,i}$  and  $D_k^a$  are listed in Tables 2-5 for the different energies and channels. Note that the overall dimensions for  $c_{AB}^{1,i}$  and  $c_{AB}^{2,i}$ ,  $i = \gamma, Z$  are GeV<sup>2</sup> and GeV respectively and that of  $\langle O_1^2 \rangle$  and  $\langle O_2^2 \rangle$  are GeV<sup>4</sup> and GeV<sup>2</sup> respectively, which for brevity, will not be mentioned in the rest of the discussion.

In order to get a feeling for the dependence of the quantities of interest on the polarization, we illustrate  $\pi\pi$  channel. In Fig. 3, we present  $c_{\pi\pi}^{1,\gamma}$  as a function of  $P_e$ . The sign of  $P_e$  is opposite to  $P_{\bar{e}}$  in order to maximize the

AB	$C_1^{1,\gamma}$	$C_2^{1,\gamma}$	$C_1^{1,Z}$	$C_2^{1,Z}$	$D_1^1$	$D_2^1$
$\pi\pi$	$2.70 \cdot 10^{-5}$	$2.94 \cdot 10^{-4}$	$-1.79 \cdot 10^{-4}$	$-2.12 \cdot 10^{-6}$	$3.27 \cdot 10^{-2}$	$7.31 \cdot 10^{-3}$
$\pi\rho$	$6.67 \cdot 10^{-6}$	$2.30 \cdot 10^{-4}$	$-1.41 \cdot 10^{-4}$	$7.22 \cdot 10^{-6}$	$2.92 \cdot 10^{-2}$	$3.28 \cdot 10^{-3}$
$\rho\rho$	$1.20 \cdot 10^{-6}$	$1.32 \cdot 10^{-4}$	$-8.08 \cdot 10^{-5}$	$5.73 \cdot 10^{-6}$	$2.47 \cdot 10^{-2}$	$1.10 \cdot 10^{-3}$

Table 2: List of coefficients for the operator  $O_1$  for  $\sqrt{s} = 500$  GeV.

AB	$C_1^{2,\gamma}$	$C_2^{2,\gamma}$	$C_1^{2,Z}$	$C_2^{2,Z}$	$D_1^2$	$D_2^2$
$\pi\pi$	$-8.61 \cdot 10^{-7}$	$6.89 \cdot 10^{-8}$	$-8.46 \cdot 10^{-8}$	$5.33 \cdot 10^{-7}$	$1.25 \cdot 10^{-2}$	$-8.77 \cdot 10^{-4}$
$\pi\rho$	$-5.92 \cdot 10^{-7}$	$4.74 \cdot 10^{-8}$	$-5.83 \cdot 10^{-8}$	$3.66 \cdot 10^{-7}$	$1.44 \cdot 10^{-2}$	$-2.38 \cdot 10^{-3}$
$\rho\rho$	$-3.24 \cdot 10^{-7}$	$2.59 \cdot 10^{-8}$	$-3.18 \cdot 10^{-8}$	$2.10 \cdot 10^{-7}$	$1.17 \cdot 10^{-2}$	$-8.17 \cdot 10^{-4}$

Table 3: List of coefficients for the operator  $O_2$  for  $\sqrt{s} = 500$  GeV.

effects of longitudinal polarization. In Fig. 4, we have an analogous illustration of  $c_{\pi\pi}^{1,Z}$ . One may note that the curvature of the profiles in Figs. 3 and 4 differ, which is dictated by the relative sizes and signs of the coefficients  $C_k^{1,i}$  that enter the final expressions for  $c_{\pi\pi}^{1,i}$ . In Fig. 5, we present profiles of the quantity  $S_1$  for the  $\pi\pi$  channel. In Fig. 6 and 7 we illustrate the behavior of  $c_{\pi\pi}^{2,\gamma}$  and  $c_{\pi\pi}^{2,Z}$ . For maximum electron polarization  $P_e = \pm 1$  all quantities become independent of  $P_e$ , since the effective polarization parameter no longer depends on  $P_e$  ( $P = \pm 1$ ). We do not illustrate the behavior of  $S_2$  since this quantity is practically constant with a value of 52.40 in the entire range of the positron polarization. We have not plotted the corresponding curves for the channels involving the  $\rho$  and these may be simply generated from the entries given in the tables.

We now discuss the limits achievable at TESLA with the design luminosities and polarizations (we give 1 standard deviation uncertainties). With a fixed value of electron and positron polarizations, one can only obtain limits on linear combinations of the EDM and WDM. Such limits would be defined by straight lines given by the equation

$$\frac{\delta \text{Red}_\tau^\gamma}{a} + \frac{\delta \text{Red}_\tau^Z}{b} = \pm 1 \quad (15)$$

for the limits arising from  $O_1$  and by

$$\frac{\delta \text{Im}d_\tau^\gamma}{c} + \frac{\delta \text{Im}d_\tau^Z}{d} = \pm 1 \quad (16)$$

for the limits arising from  $O_2$  where the numbers  $a$ ,  $b$ ,  $c$ , and  $d$  can be explicitly computed for given polarizations and luminosities. The value of  $a$



AB	$C_1^{1,\gamma}$	$C_2^{1,\gamma}$	$C_1^{1,Z}$	$C_2^{1,Z}$	$D_1^1$	$D_2^1$
$\pi\pi$	$1.65 \cdot 10^{-5}$	$1.84 \cdot 10^{-4}$	$-1.10 \cdot 10^{-4}$	$-1.09 \cdot 10^{-6}$	$3.26 \cdot 10^{-2}$	$7.17 \cdot 10^{-3}$
$\pi\rho$	$4.08 \cdot 10^{-6}$	$1.44 \cdot 10^{-4}$	$-8.64 \cdot 10^{-5}$	$4.47 \cdot 10^{-6}$	$2.92 \cdot 10^{-2}$	$3.22 \cdot 10^{-3}$
$\rho\rho$	$7.35 \cdot 10^{-7}$	$8.22 \cdot 10^{-5}$	$-4.95 \cdot 10^{-4}$	$3.52 \cdot 10^{-6}$	$2.46 \cdot 10^{-2}$	$1.10 \cdot 10^{-3}$

Table 4: List of coefficients for the operator  $O_1$  for  $\sqrt{s} = 800$  GeV.

AB	$C_1^{2,\gamma}$	$C_2^{2,\gamma}$	$C_1^{2,Z}$	$C_2^{2,Z}$	$D_1^2$	$D_2^2$
$\pi\pi$	$-3.29 \cdot 10^{-7}$	$2.63 \cdot 10^{-8}$	$-3.17 \cdot 10^{-8}$	$2.00 \cdot 10^{-7}$	$1.25 \cdot 10^{-2}$	$-8.54 \cdot 10^{-4}$
$\pi\rho$	$-2.26 \cdot 10^{-7}$	$1.81 \cdot 10^{-8}$	$-2.18 \cdot 10^{-8}$	$1.37 \cdot 10^{-7}$	$1.43 \cdot 10^{-2}$	$-2.32 \cdot 10^{-3}$
$\rho\rho$	$-1.24 \cdot 10^{-7}$	$9.92 \cdot 10^{-9}$	$-1.19 \cdot 10^{-8}$	$7.51 \cdot 10^{-8}$	$1.16 \cdot 10^{-2}$	$-7.96 \cdot 10^{-4}$

Table 5: List of coefficients for the operator  $O_2$  for  $\sqrt{s} = 800$  GeV.

( $c$ ) is the sensitivity to the real (imaginary) part of the EDM when the real (imaginary) part of the WDM is set to zero and  $b$  ( $d$ ) is the sensitivity to the WDM when the EDM is set to zero.

The quantities  $a$ ,  $b$ ,  $c$ , and  $d$  are plotted in Figs. 8-11 as functions of  $P_e$  in the vicinity of  $P_e = -0.8$ , for the reference values of  $P_{\bar{e}}$ . In all cases, the variation with  $P_e$  and  $P_{\bar{e}}$  is slow in the range we have chosen, since we are already close to the maximum effective polarization. Many models predict a significantly larger EDM than WDM. In this case the limits achievable are precisely  $a$  and  $c$  on the real and imaginary parts of the EDM. If this is not the case, the EDM and WDM can be disentangled by switching the relative signs of  $P_e$  and  $P_{\bar{e}}$ . The limits achievable for equal luminosities for both settings are given in Tab. 6. The pairs  $(\mathcal{A}, \mathcal{B})$  and  $(-\mathcal{A}, -\mathcal{B})$  give the vertices in the  $\text{Re } d_\tau^\gamma$ - $\text{Re } d_\tau^Z$  plane and  $(\mathcal{C}, \mathcal{D})$  and  $(-\mathcal{C}, -\mathcal{D})$  in the analogous  $\text{Im } d_\tau^\gamma$ - $\text{Im } d_\tau^Z$  plane.

We also present below a table of numbers computed for the contribution from the helicity flip bremsstrahlung to the operator  $O_2$ . We schematically express it as

$$\langle O_2 \rangle_{SM} = \frac{-A'(P_e + P_{\bar{e}})}{\sigma_1(1 - P_e P_{\bar{e}}) + \sigma_2(P_e - P_{\bar{e}})} \quad (17)$$

where the quantity  $\langle O_2 \rangle_{SM}$  has the overall dimension of GeV, and the corresponding coefficient  $A'$  is tabulated in Tab. 7. The cross-sections  $\sigma_i$  are given in Tab. 1. Even with extreme values of  $P_e$  and  $P_{\bar{e}}$ , we get a number of order 1, to be contrasted with  $S_2 \simeq 50$  for the  $\pi\pi$  channel thereby rendering this background negligible.

$\sqrt{s}$ GeV	$\mathcal{A}$	$\mathcal{B}$	$\mathcal{C}$	$\mathcal{D}$
500	$3.73 \cdot 10^{-20}$	$-5.90 \cdot 10^{-19}$	$-9.31 \cdot 10^{-17}$	$3.15 \cdot 10^{-18}$
	$-3.84 \cdot 10^{-19}$	$1.03 \cdot 10^{-20}$	$1.05 \cdot 10^{-17}$	$-1.60 \cdot 10^{-16}$
800	$2.63 \cdot 10^{-20}$	$-4.25 \cdot 10^{-19}$	$-1.07 \cdot 10^{-16}$	$3.90 \cdot 10^{-18}$
	$-2.71 \cdot 10^{-19}$	$7.39 \cdot 10^{-21}$	$1.22 \cdot 10^{-17}$	$-1.88 \cdot 10^{-16}$

Table 6: Sensitivities achievable when signs of electron and positron polarizations are interchanged.

AB	$\sqrt{s}=500$ GeV	$\sqrt{s}=800$ GeV
$\pi\pi$	338	243
$\pi\rho$	343	242
$\rho\rho$	349	241

Table 7: Coefficient  $A'$  of helicity-flip bremsstrahlung to  $\langle O_2 \rangle_{SM}$ .

TESLA can also be operated at the Z-pole. It is expected that sufficient integrated luminosity will be available to generate as many as  $10^9$  Z bosons. A simple scaling of the limits obtained in ref. [11] with the effective polarization parameter  $P \simeq 0.95$  could yield 1 s.d. limits of  $3 \times 10^{-19}$  e-cm on the real part, and  $10^{-18}$  e-cm on the imaginary part of the weak dipole moment.

## 5 Experimental Aspects

Up to this point we have done analytic calculations of vector correlations for two decay channels of the  $\tau$  lepton. This gives us a realistic estimate of the limits that can be achieved on the EDM and WDM with these decays with a perfect detector. Here we want to discuss possibilities of improving the sensitivity further and we try to estimate by how much the result will be weakened due to detector effects in a real experiment. We will try to extrapolate the size of the detector effects from the experience from the LEP experiments and SLD [13].

- In the calculations we have taken into account the decays into  $\pi$  and  $\rho$ . These are the two most important channels. Together they make up 13 % of the total branching ratio of  $\tau$  pairs. More channels can be added. The decay modes  $\tau^- \rightarrow \pi^- \pi^+ \pi^- \nu_\tau$  and  $\tau^- \rightarrow \pi^- \pi^0 \pi^0 \nu_\tau$  and the two leptonic decays  $\tau^- \rightarrow e^- \bar{\nu}_e \nu_\tau$  and  $\tau^- \rightarrow \mu^- \bar{\nu}_\mu \nu_\tau$  have been used at LEP/SLC. This increases the potential fraction of the

sample used in the analysis to 82 %. However, these additional channels have a lower sensitivity to CP violation. Taking this into account the theoretically achievable sensitivity increased by a factor of 2.8 at the Z-pole. There will probably be a similar factor at TESLA.

- The vector correlations discussed here receive contributions from the most important part of the cross-section. They are more sensitive than the tensor correlations initially discussed in [14], if beam polarization is available. With so-called optimal observables [15] the sensitivity from every part of the cross-section can be exploited. The experiments at LEP/SLC started off using the tensor correlations. When they later moved to the optimal observables, the sensitivity improved by roughly an order of magnitude. Also here we expect a gain in sensitivity from the optimal observables, although the situations are not directly comparable.
- The real detector will have a finite energy and momentum resolution for the decay products of the  $\tau$  leptons. This affects the calculation of the observables and reduces the sensitivity. The reduction of sensitivity at LEP/SLC was less than 10 % for events without  $\pi^0$  in the final state and in the order of 10 % for events with  $\pi^0$  mesons. Despite the higher energies, the relative momentum resolution of the TESLA detector for charged particles should be slightly better than that at LEP/SLC. The energy resolution of the  $\pi^0$ s (causing the main loss of sensitivity at LEP/SLC) should be substantially better at TESLA. We assume that the loss of sensitivity due to finite energy and momentum resolution will not be larger than 10 %.
- In a real experiment the event samples selected will contain background from misidentified  $\tau$  decays and also from non  $\tau$  pair events. The background dilutes the signal and reduces the sensitivity. This reduction of sensitivity was between 1 and 10 percent at LEP/SLC for the different decay channels. At higher center-of-mass energies at TESLA the higher Lorentz boost of the  $\tau$  leptons makes the identification of their decay channels more difficult. But then we also expect the TESLA detector to have a better performance. Especially the high granularity of the proposed silicon-tungsten electromagnetic calorimeter will simplify  $\tau$  analysis. Overall we don't expect to lose more than 10 % in sensitivity due to background.
- The real detector will not have 100 % efficiency in the identification of the signal. At LEP/SLC typical values for the overall efficiencies

ranged between 50 and 90 % for the various decay modes of the  $\tau$  pairs. The TESLA detector should perform at least as good as the LEP/SLC detectors.

Without a detailed study based on a full analysis of events with full detector simulation it is impossible to tell by how much the limit achievable in the real experiment will differ from our analytic estimate. From the argument above we conclude that the achievable limit will not be worse than our analytic estimate. It will probably be better by a factor of a few.

## 6 Discussion and Conclusions

In the present work, we have considered vector correlations among the momenta of charged decay products of the  $\tau^\pm$  in two-body decays into final states with  $\pi$  and  $\rho$ . By considering CP-odd operators which are T-odd ( $O_1$ ) and T-even ( $O_2$ ) it is possible to probe the real and imaginary parts of CP violating dipole form factors of the  $\tau$  lepton. We expect the following precision (1 standard deviations) with the expected beam polarizations of  $-80$  % for the electron beam and  $60$  % for the positron beam (in units of e-cm).

$\sqrt{s}$	$\int dt \mathcal{L}$	$\text{Re } d_\tau^\gamma$	$\text{Im } d_\tau^\gamma$	$\text{Re } d_\tau^Z$	$\text{Im } d_\tau^Z$
500 GeV	500 fb $^{-1}$	$3.8 \cdot 10^{-19}$	$0.9 \cdot 10^{-16}$	$5.4 \cdot 10^{-19}$	$1.4 \cdot 10^{-16}$
800 GeV	1000 fb $^{-1}$	$2.7 \cdot 10^{-19}$	$1.1 \cdot 10^{-16}$	$3.9 \cdot 10^{-19}$	$1.7 \cdot 10^{-16}$

In these determinations the limits on the electric dipole moment are obtained assuming the weak dipole moment is zero and vice-versa. It is possible to disentangle the individual limits by switching the beam polarizations (see Tab. 6).

A priori it cannot be said by how much better tensor correlations of the type considered in [2] will fare when polarization is included and conclusions cannot be drawn unless they are fully studied. However, it must be noted that the sensitivities we have reported here are significantly superior to those obtainable from the tensor correlations with no beam polarization.

The vector correlations are significantly enhanced due to longitudinal polarization of the beams. The precision achievable without polarization would be at least an order of magnitude reduced. Since the effective polarization parameter is already close to unity with the designed electron polarization alone, the gain from positron polarization even at  $60$  % improves the sensitivity by a factor of 2 at most. The measurements are not very sensitive to the precise value of the polarizations. A control on the polarization at the level of a few percent is sufficient.

## 7 Acknowledgments

It is our pleasure to thank Prof. O. Nachtmann for valuable discussions.

## References

- [1] W. Bernreuther, G. W. Botz, O. Nachtmann and P. Overmann, Z. Phys. C **52** (1991) 567.
- [2] W. Bernreuther, O. Nachtmann and P. Overmann, Phys. Rev. D **48** (1993) 78.
- [3] Y. S. Tsai, Phys. Rev. D **4**, 2821 (1971), [Erratum-ibid. **13**, 771 (1976)].
- [4] TESLA Technical Design Report Part I-VI, DESY 2001-011
- [5] G. Moortgat-Pick and H. M. Steiner, Eur. Phys. J. directC **6**, 1 (2001) [arXiv:hep-ph/0106155],  
S.D. Rindani, to appear in *Proceedings of the 4th ACFA Workshop on Physics/Detector at the Linear Collider*, Beijing, 2001 [arXiv:hep-ph/0202045],  
S.D. Rindani, *Proceedings of the Theory Workshop on Physics at Linear Colliders*, Tsukuba, 2001, [arXiv:hep-ph/0105318].
- [6] B. Ananthanarayan and S. D. Rindani, Phys. Rev. D **52** (1995) 2684.
- [7] W. Bernreuther and M. Suzuki, Rev. Mod. Phys. **63**, 313 (1991) [Erratum-ibid. **64**, 633 (1991)].
- [8] F. Hoogeveen, Nucl. Phys. B **341** (1990) 322.
- [9] W. Bernreuther, A. Brandenburg and P. Overmann, Phys. Lett. B **391** (1997) 413.
- [10] P. Poulose and S. D. Rindani, Pramana **51** (1998) 387.
- [11] B. Ananthanarayan and S. D. Rindani, Phys. Rev. Lett. **73** (1994) 1215;  
B. Ananthanarayan and S. D. Rindani, Phys. Rev. D **50** (1994) 4447.
- [12] B. Ananthanarayan and S. D. Rindani, Phys. Rev. D **51** (1995) 5996.
- [13] ALEPH, D. Buskulic *et al.*, Phys. Lett. B **346**, 371 (1995),  
L3, M. Acciarri *et al.*, Phys. Lett. B **426**, 207 (1998),  
OPAL, K. Ackerstaff *et al.*, Z. Phys. C **74**, 403 (1997),  
SLD, K. Abe *et al.*, SLAC-PUB-8163.

- [14] W. Bernreuther, U. Low, J. P. Ma and O. Nachtmann, *Z. Phys. C* **43**, 117 (1989),  
W. Bernreuther and O. Nachtmann, *Phys. Rev. Lett.* **63**, 2787 (1989)  
[Erratum-ibid. **64**, 1072 (1989)],  
W. Bernreuther and O. Nachtmann, *Phys. Lett. B* **268**, 424 (1991),  
W. Bernreuther, G. W. Botz, O. Nachtmann and P. Overmann, *Z. Phys. C* **52** (1991) 567.
- [15] P. Overmann, *A New method to measure the tau polarization at the Z peak*, University of Dortmund, DO-TH-93-24,  
D. Atwood and A. Soni, *Phys. Rev. D* **45**, 2405 (1992),  
M. Diehl and O. Nachtmann, *Z. Phys. C* **62**, 397 (1994).

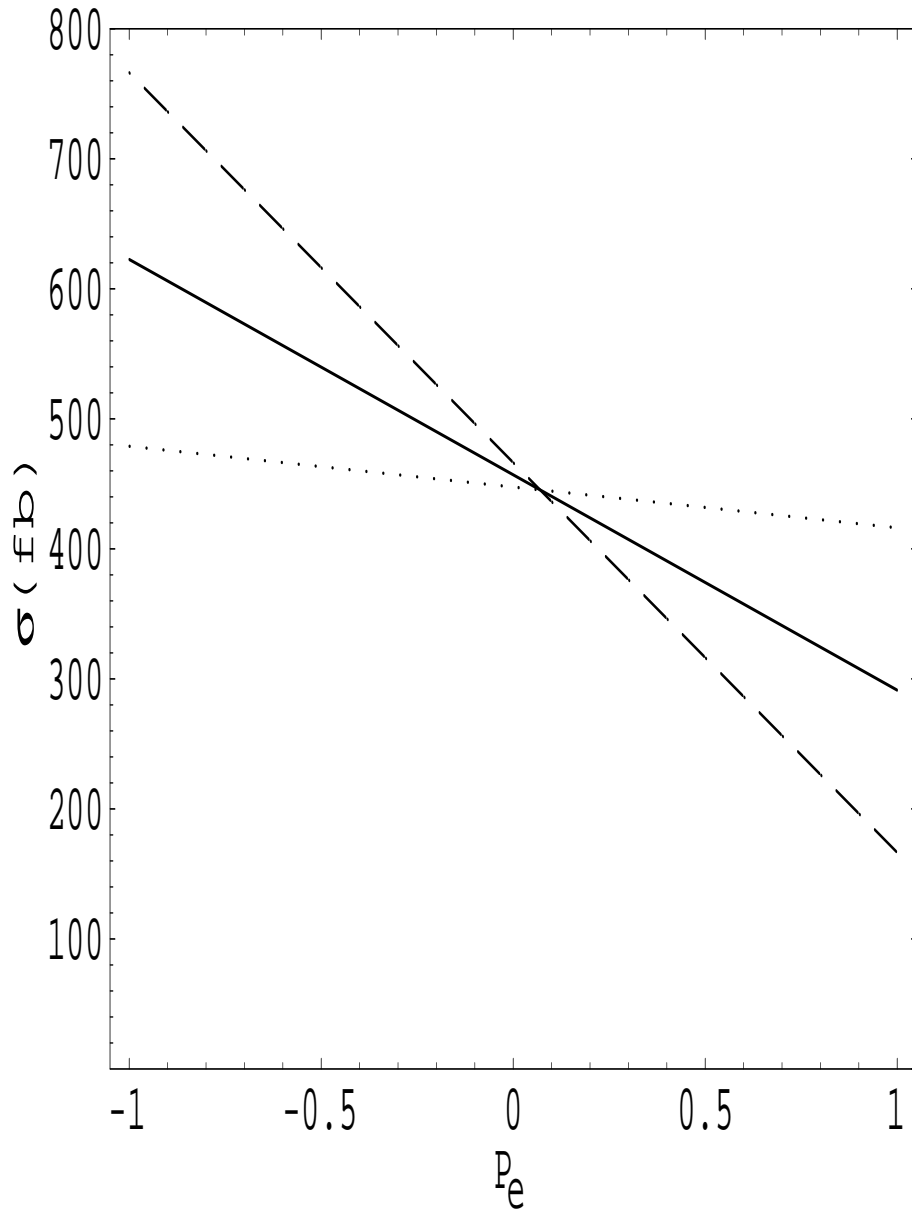


Figure 1: Values of the cross-section for  $P_e = 0, 0.3, 0.6$  (dotted, solid and dashed) as a function of  $P_e$ , with  $\sqrt{s} = 500$  GeV.

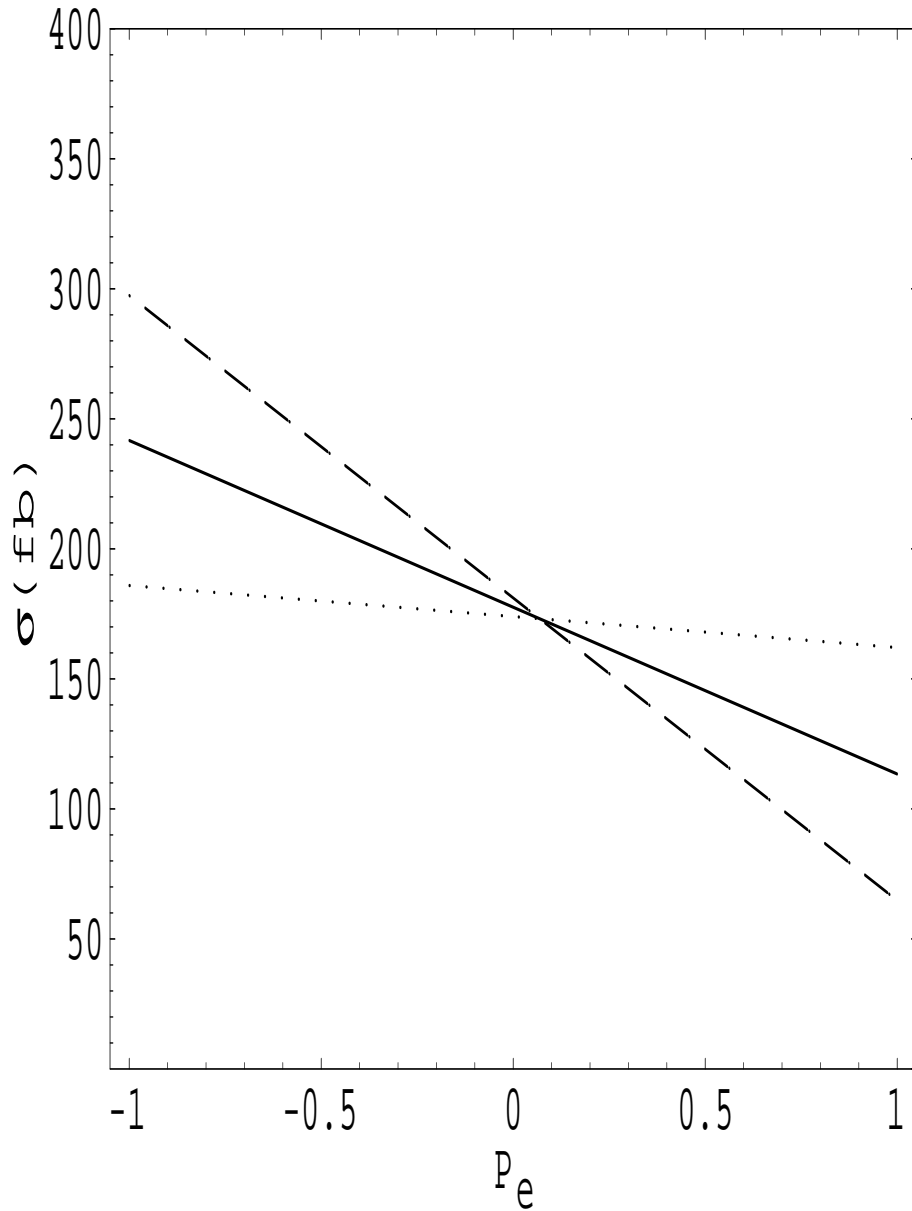


Figure 2: Values of the cross-section for  $P_e = 0, 0.3, 0.6$  (dotted, solid and dashed) as a function of  $P_e$ , with  $\sqrt{s} = 800$  GeV.



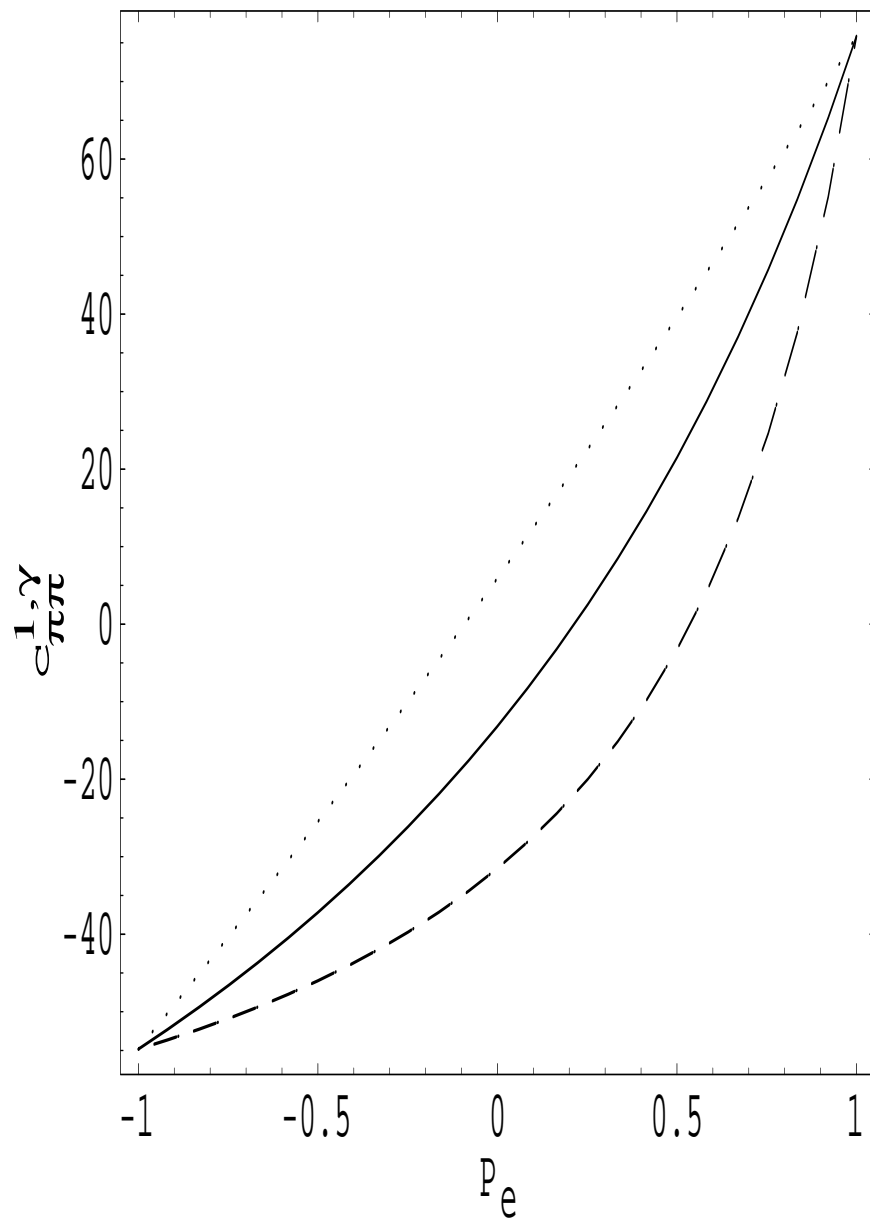


Figure 3: Values of  $c_{\pi\pi}^{1,\gamma}$  for  $P_e = 0, 0.3, 0.6$  (dotted, solid and dashed) as a function of  $P_e$ , with  $\sqrt{s} = 500$  GeV.

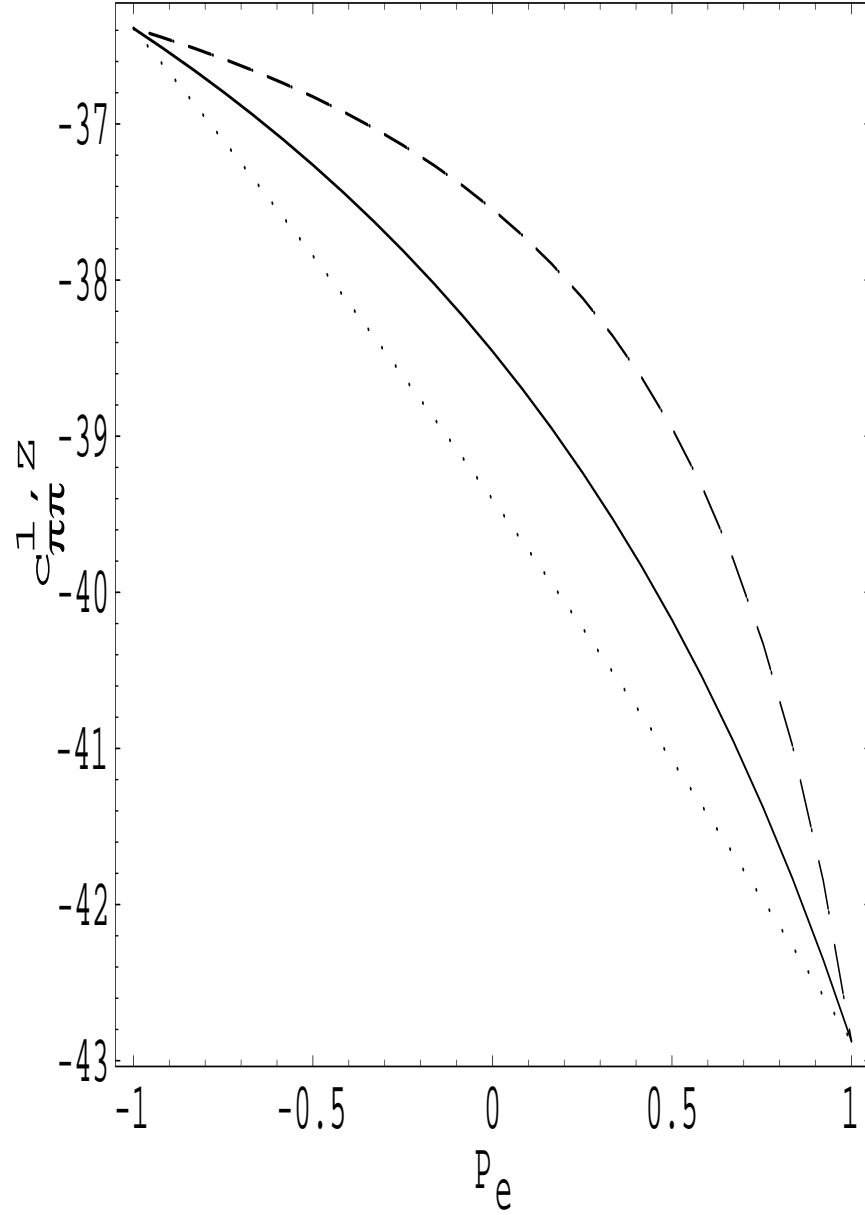


Figure 4: Values of  $c_{\pi\pi}^{1,Z}$  for  $P_e = 0, 0.3, 0.6$  (dotted, solid and dashed) as a function of  $P_e$ , with  $\sqrt{s} = 500$  GeV.

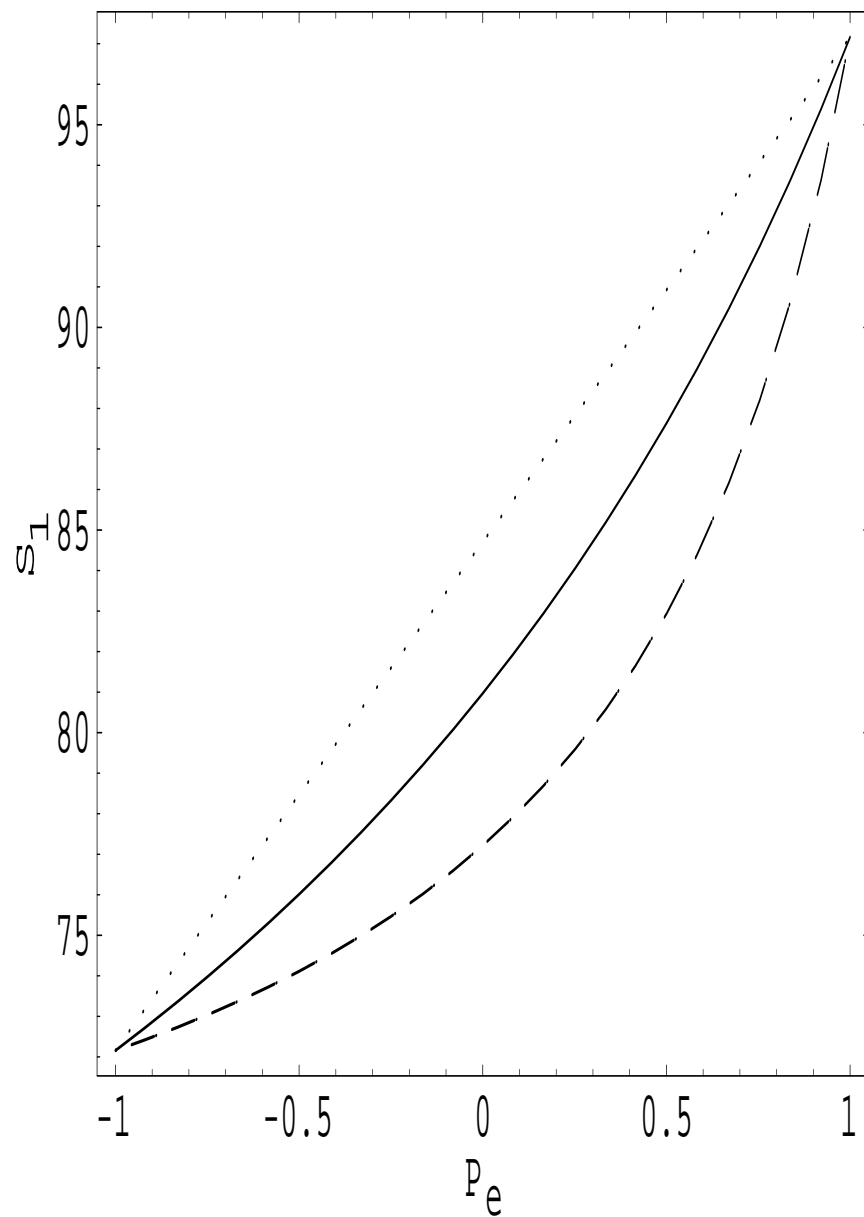


Figure 5: Values of  $S_1$  for  $P_e = 0, 0.3, 0.6$  (dotted, solid and dashed) as a function of  $P_e$ , with  $\sqrt{s} = 500$  GeV.

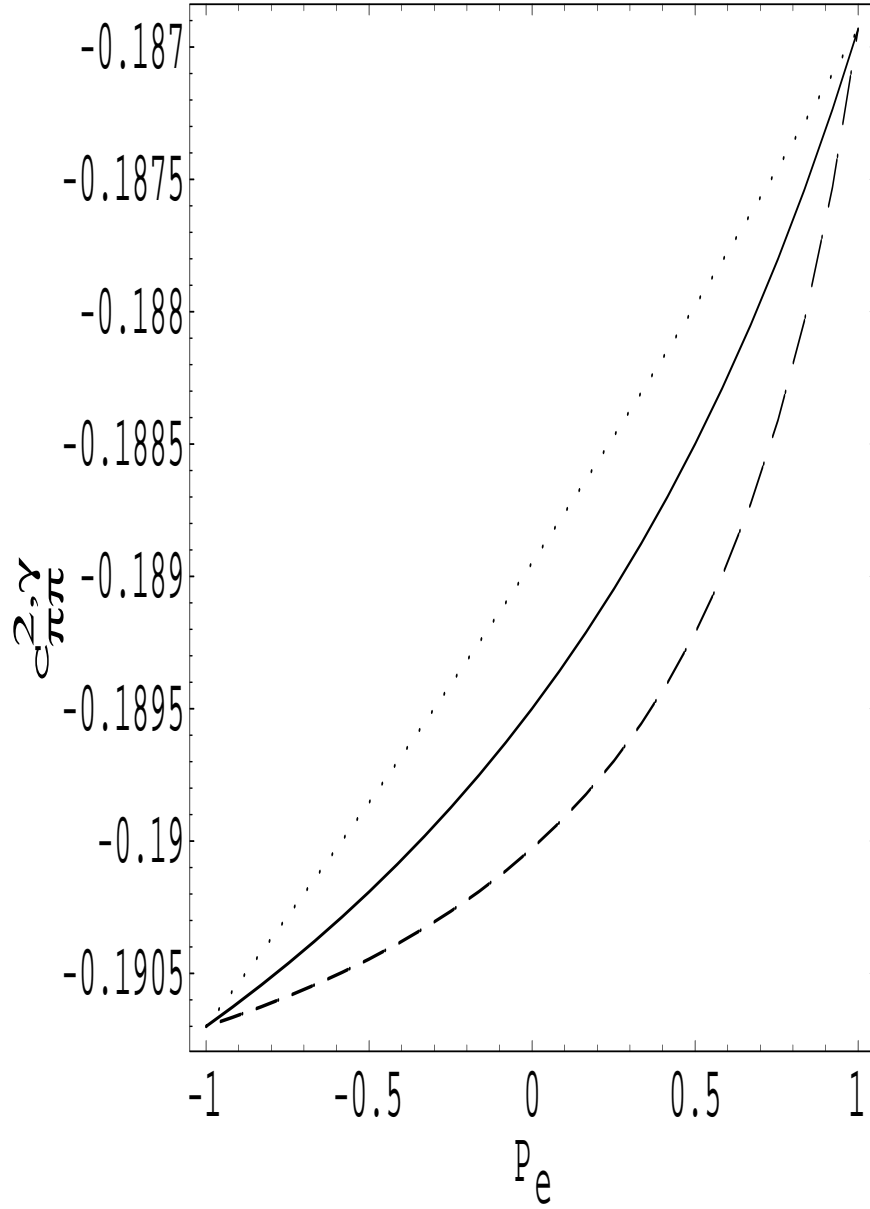


Figure 6: Values of  $c_{\pi\pi}^{2,\gamma}$  for  $P_{\bar{e}} = 0, 0.3, 0.6$  (dotted, solid and dashed) as a function of  $P_e$ , with  $\sqrt{s} = 500$  GeV.

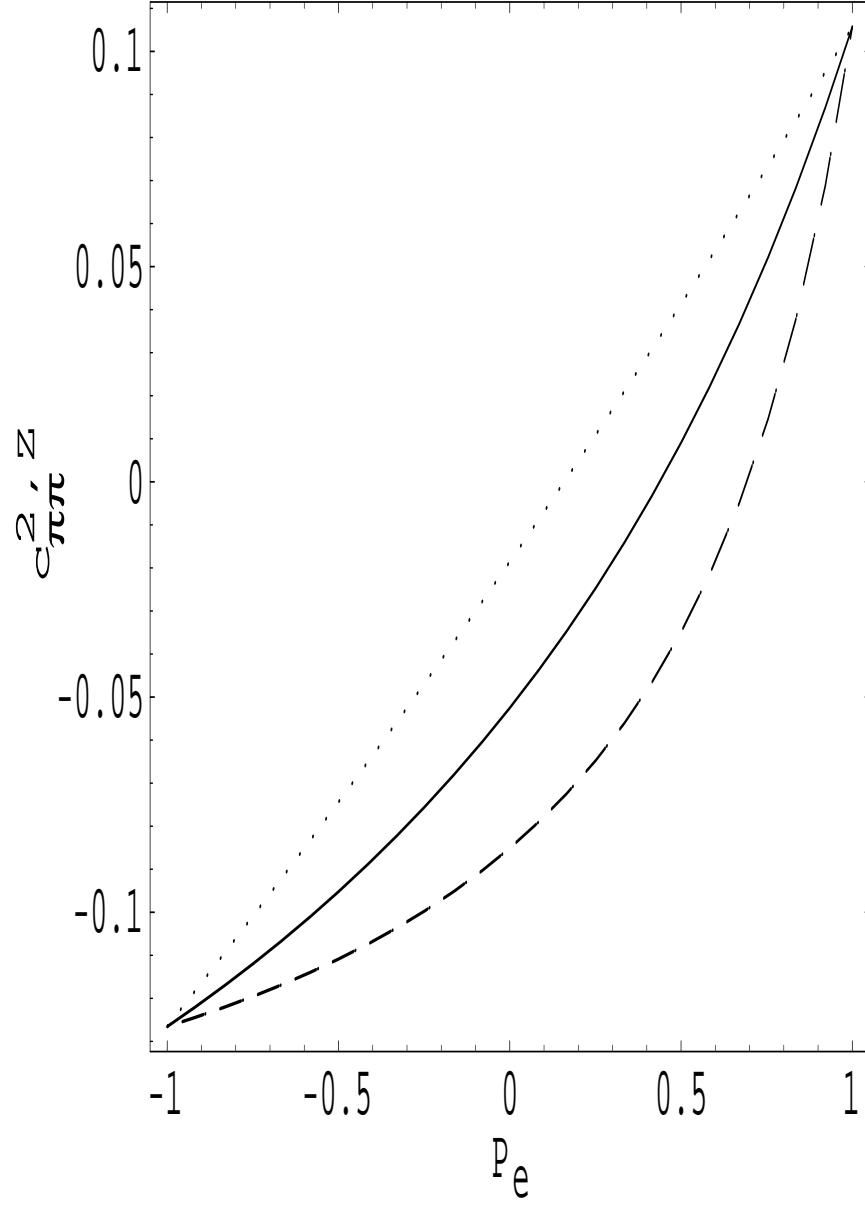


Figure 7: Values of  $c_{\pi\pi}^{2,Z}$  for  $P_e = 0, 0.3, 0.6$  (dotted, solid and dashed) as a function of  $P_e$ , with  $\sqrt{s} = 500$  GeV.

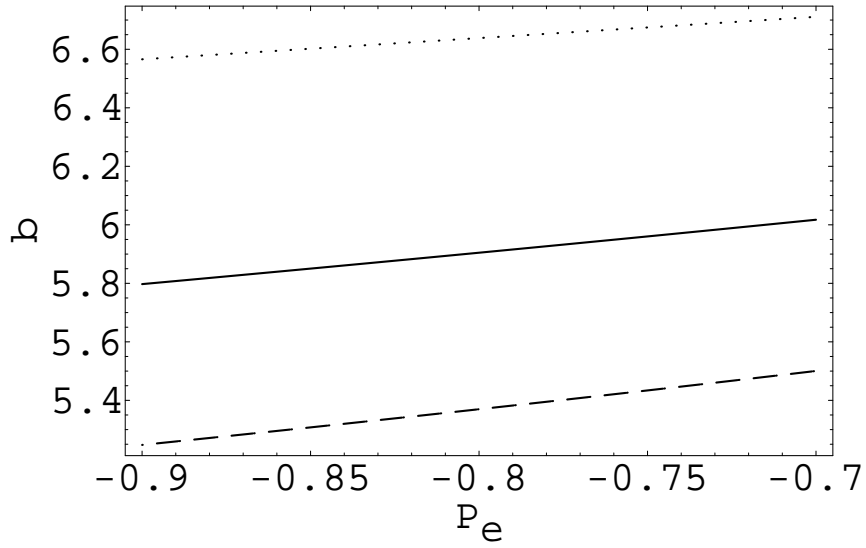
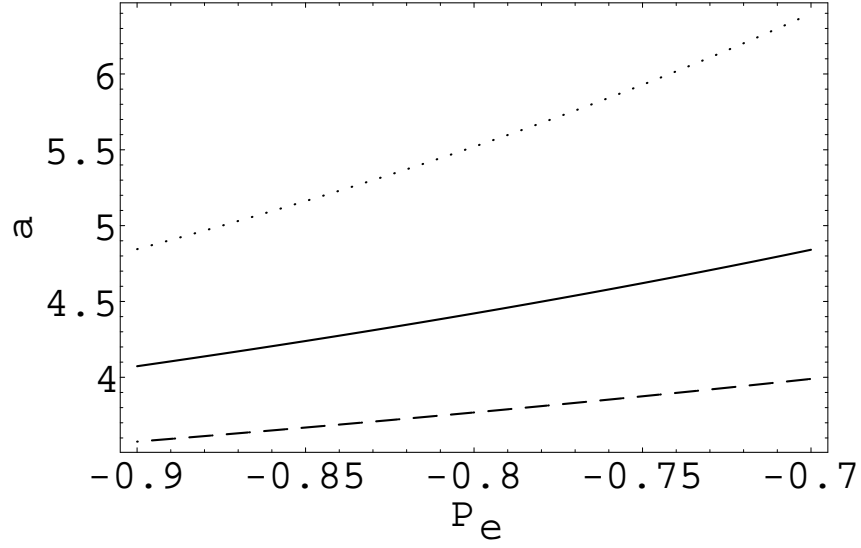


Figure 8: Values of  $a$  and  $b$  (in units of  $10^{-19}$  e-cm) for  $P_e = 0, 0.3, 0.6$  (dotted, solid and dashed) as a function of  $P_e$  in the vicinity of the expected value of  $-0.8$  for  $\int dt \cdot \mathcal{L} = 500 \text{ fb}^{-1}$  and  $\sqrt{s} = 500 \text{ GeV}$ .

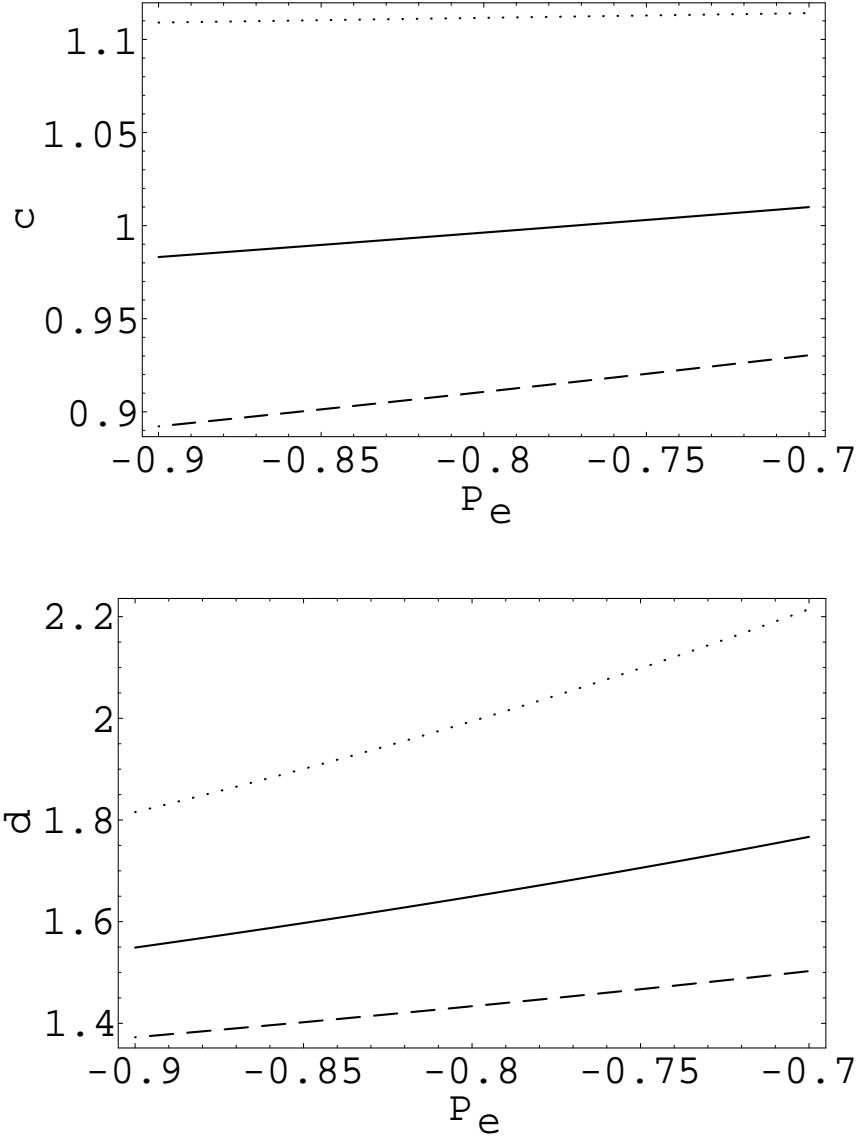


Figure 9: Values of  $c$  and  $d$  (in units of  $10^{-16}$  e-cm) for  $P_{\bar{e}} = 0, 0.3, 0.6$  (dotted, solid and dashed) as a function of  $P_e$  in the vicinity of the expected value of  $-0.8$  for  $\int dt \cdot \mathcal{L} = 500 \text{ fb}^{-1}$  and  $\sqrt{s} = 500 \text{ GeV}$ .

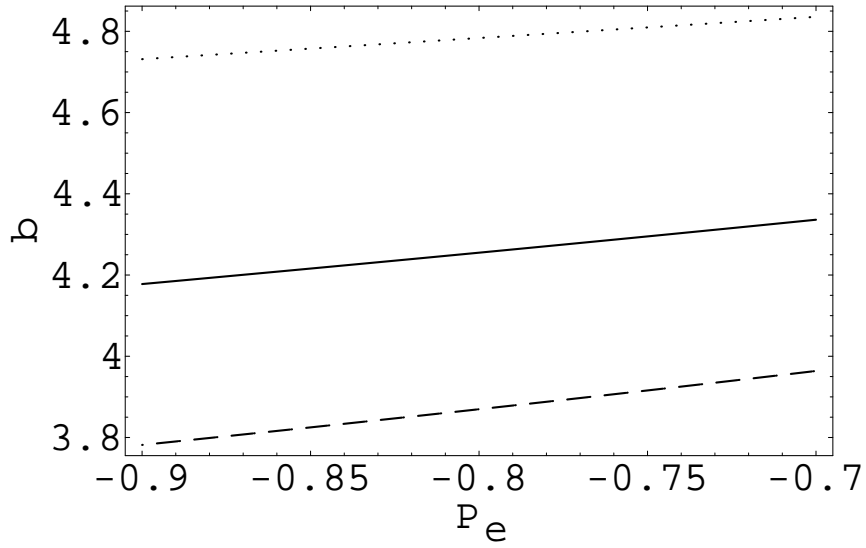
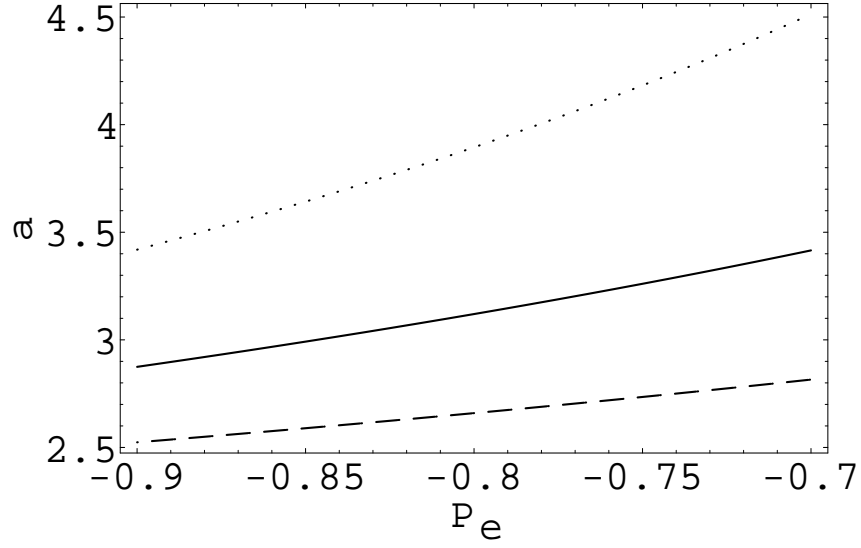


Figure 10: Values of  $a$  and  $b$  (in units of  $10^{-19}$  e-cm) for  $P_e = 0, 0.3, 0.6$  (dotted, solid and dashed) as a function of  $P_e$  in the vicinity of the expected value of  $-0.8$  for  $\int dt \cdot \mathcal{L} = 1000 \text{ fb}^{-1}$  and  $\sqrt{s} = 800 \text{ GeV}$ .



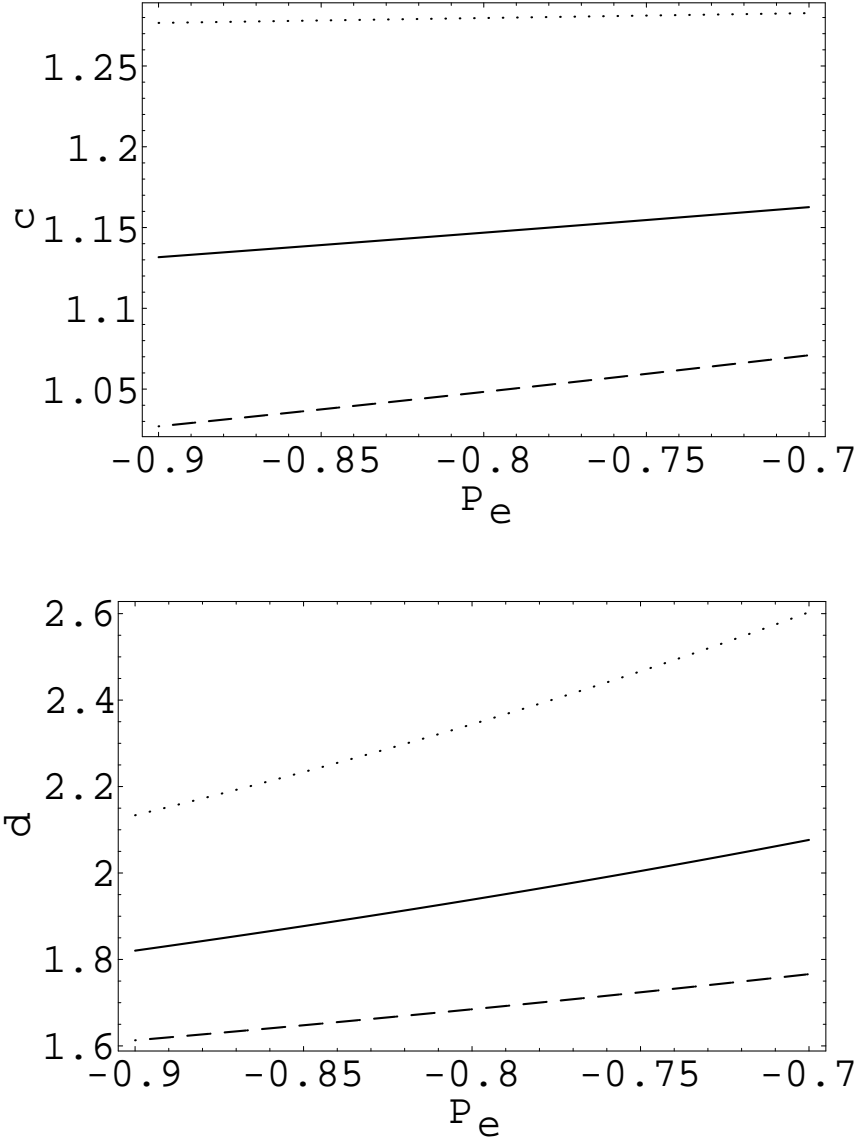


Figure 11: Values of  $c$  and  $d$  (in units of  $10^{-16}$  e-cm) for  $P_{\bar{e}} = 0, 0.3, 0.6$  (dotted, solid and dashed) as a function of  $P_e$  in the vicinity of the expected value of  $-0.8$  for  $\int dt \cdot \mathcal{L} = 1000 \text{ fb}^{-1}$  and  $\sqrt{s} = 800 \text{ GeV}$ .